Structural Effects of a Basic Peptide on the Organization of Dipalmitoylphosphatidylcholine/Dipalmitoylphosphatidylserine Membranes: A Fluorescent Resonance Energy Transfer Study

Luís M. S. Loura,*,†,‡ Ana Coutinho,†,§ Ana Silva,†,|| Aleksander Fedorov,† and Manuel Prieto†

Centro de Química-Física Molecular, Complexo I, Instituto Superior Técnico, Av. Rovisco Pais, P-1049-001 Lisboa, Portugal, Centro e Departamento de Química, Universidade de Évora, R. Romão Ramalho, 59, P-7000-671 Évora, Portugal, and Departamento de Química e Bioquímica, Bloco C8, Faculdade de Ciências, Universidade de Lisboa, R. Ernesto de Vasconcelos, P-1749-016 Lisboa, Portugal

Received: October 13, 2005; In Final Form: March 2, 2006

We studied the effect of a model basic peptide, hexalysiltryptophan, on the organization of dipalmitoylphosphatidylcholine/dipalmitoylphosphatidylserine unilamellar vesicles by means of fluorescent resonance energy transfer (FRET) between fluorescently labeled phospholipids. Several FRET theoretical models assuming different bilayer geometries and probe distributions were fitted to the time-resolved data. The experiments were carried out at two temperatures in different regions of the lipid mixture phase diagram. At 45 °C, the expected gel/fluid phase separation was verified by model fitting in peptide-free vesicles, which from the FRET approach means that domains are larger than ∼200 Å. No noticeable alteration of membrane organization was detected upon increasing the peptide concentration. At variance, for the single fluid phase at 60 °C, there was a large increase in FRET efficiency upon peptide addition to the lipid vesicles, mainly caused by peptide-induced vesicle aggregation. The system gradually changed from unilamellar lipid vesicles to a multibilayer geometry, and a limit lamellar repeat distance of ∼57 Å was recovered. Furthermore, no evidence for lateral domain formation on the FRET length scale was found at this temperature, the cationic peptide being only able to induce local lipid demixing, causing a short-range sequestration of 2−3 acidic lipids around each surface-adsorbed peptide.

Introduction

Many proteins that are involved in cell signaling and membrane trafficking are conditional peripheral or amphitropic proteins that become reversibly attached to the membrane interface as a result of interaction of a modular membrane-targeting protein domain with specific lipids in the membranes.[1,2] Acidic phospholipids located in the inner leaflet of plasma membranes are one of the targeted species[3] because they often promote membrane binding of several protein modules, such as C2 and pleckstrin homology (PH) domains, via electrostatic interactions between the negatively charged lipid headgroups (phosphatidylserine (PS) and phosphoinositides, respectively) and clusters of basic groups on the proteins.

The possibility that protein binding can trigger the formation of lateral domains in mixed lipid membranes, composed of negatively charged and neutral lipids, has long been a subject of interest in membrane biophysics,[4−6] and experimental evidence for this kind of lipid segregation has been reported for various systems.[7−10] Formation of domains of lipid minor components may play a crucial role in signal amplification by providing platforms for assembly of protein complexes.[11]

In addition to lipid clustering thermodynamically coupled to protein binding, membrane aggregation and/or fusion are also known to be common occurrences when studying the interaction of cationic agents, such as mono- and divalent cations[12] or basic peptides,[13,14] with negatively charged membranes. These effects may complicate data interpretation[15,16] because addition of the cationic agents to the liposomes can cause profound alterations in the morphology of the lipid vesicles.[17−20] To understand the factors that regulate the formation, stability, and dynamics of basic peptide-induced lipid domains, it is therefore important to fully characterize the effects of these cationic agents on membrane organization, which depend on the cationic species and concentration as well as on the membrane composition.

The purpose of the present work was to study the ability of a model peptide (Lys_6Trp or K_6W) to reorganize two-component lipid bilayers containing a zwitterionic phospholipid, 1,2-dipalmitoyl-*sn*-glycero-3-phosphocholine (DPPC), and an acidic one, 1,2-dipalmitoyl-*sn*-glycero-3-phosphoserine (DPPS). K_6W was selected as a model for the small basic amino acid clusters found in a variety of cytoplasmic membrane-associating proteins, and a Trp residue was included in the peptide sequence to allow for the use of fluorescence techniques in monitoring peptide interaction with the phospholipid vesicles. The DPPC/DPPS system was chosen because (i) diacylphosphatidylcholines are the major phospholipid components of eukaryotic plasma membranes and diacylphosphatidylserines are the most common anionic phospholipids present in the inner leaflet of these membranes and (ii) it has the advantage of exhibiting a large gel/fluid phase coexistence range due to its nonideal mixing properties. Thus, experiments can be carried out in both two-phase (i.e., between the *solidus* and *liquidus* lines in the phase

* Author to whom correspondence should be addressed. E-mail: pclloura@alfa.ist.utl.pt. Phone: +351218419219. Fax: +351218464455.
† Instituto Superior Técnico.
‡ Universidade de Évora.
§ Universidade de Lisboa.
|| Present address: Instituto Gulbenkian de Ciência, Rua da Quinta Grande, 6, P-2780-156 Oeiras, Portugal

10.1021/jp055855i CCC: $30.25
Published on Web 03/29/2006

diagram) and single-phase (above the *liquidus* line) systems; i.e., the influence of preformed acidic domains upon peptide interaction with the lipid vesicles can be investigated. We sought information regarding the eventual ability of the fluorescent basic peptide to cause membrane reorganization, either by inducing (i) vesicle aggregation and/or (ii) lateral segregation of lipids (in the nanometer length scale and nanosecond time scale), for both fluid vesicles and vesicles in the gel/fluid coexistence range.

To this effect, we used fluorescence resonance energy transfer (FRET) (for a review, see ref 21), which is particularly suited for probing these two distinct phenomena. The effect of peptide addition to two-component membranes is easily monitored by the variation of FRET efficiency between a convenient pair of fluorescent probes (which mimic the nonfluorescent lipid components). For example, if the FRET donor and acceptor probes mimic one of the lipid mixture components, then peptide-induced phase separation leads to increased probe colocalization and consequently to enhanced FRET efficiency and conversely for probes that mimic different components of the lipid mixture. Literature studies have taken advantage of this effect in steady-state FRET experiments, mostly in a qualitative manner.[22,23] Independently, an increase in FRET efficiency may also arise from vesicle aggregation, as additional planes of acceptor molecules become available (i.e., closer than $\sim 2R_0$, the Förster radius) for quenching of donor fluorescence. We show by judicial analysis of time-resolved fluorescence data (at variance with the more common steady-state approach) that the two potential effects (vesicle aggregation and lateral phase separation) can be discriminated in the same experiment, and quantitative topological and topographical information regarding the interaction of a peptide with the model membranes may be recovered.

FRET Theoretical Background

The kinetics of FRET was originally derived by Förster.[24] The rate of energy transfer between a donor molecule, D, with fluorescence lifetime τ, and an acceptor molecule, A, separated by a distance R, is given by

$$k_T = \frac{1}{\tau}\left(\frac{R_0}{R}\right)^6 \tag{1}$$

where R_0 is the critical distance or Förster radius, which can be calculated from

$$R_0 = 0.2108 \times [\kappa^2 \Phi_D n^{-4} J(\lambda)]^{1/6} \tag{2}$$

In this equation, κ^2 is the orientation factor (see ref 25 for a detailed discussion), Φ_D is the donor quantum yield in the absence of acceptor, n is the refractive index, λ is the wavelength, and $J(\lambda)$ is the spectral overlap integral between the emission spectrum of the donor, $I_D(\lambda)$, and the molar absorption spectrum of the acceptor, $\epsilon_A(\lambda)$, given by

$$J = \frac{\int I_D(\lambda)\epsilon_A(\lambda)\lambda^4 \, d\lambda}{\int I_D(\lambda) \, d\lambda} \tag{3}$$

If the λ units used in eq 3 are nanometers, then the calculated R_0 in eq 2 has Å units.

In the case where the donor molecules are surrounded by a uniform distribution of acceptors, the donor decay law becomes complex.[21] The result for an infinite two-dimensional system (or any system with donors and acceptors in the same plane, cis transfer), assuming that (i) there is no homotransfer between donors, (ii) the fraction of excited acceptors is negligible, (iii) translational diffusion is negligible, and (iv) the exclusion distance between donors and acceptors is much smaller than R_0, is

$$i_{DA,cis}^{uniform}(t) = i_D(t) \exp(-C(t/\tau)^{1/3}) \tag{4}$$

where

$$C = \Gamma(^2/_3) n \pi R_0^{\,2} \tag{5}$$

and $i_D(t)$ is the donor decay in the absence of acceptor. In this equation, n is the surface density of acceptors and Γ is the complete gamma function.

If donors and acceptors are located in infinite parallel planes (trans transfer, as in lipid bilayers for chromophores located at different depths) and, in particular, if donors are surrounded by *two* equivalent planes of acceptors, each separated from that of the donors by a distance h_1 (Figure 1A), then the result is[26]

$$i_{DA,trans}^{uniform}(t) = i_D(t) \exp(-2kCh_1^{\,2}F(h_1,t)) \tag{6}$$

where

$$F(h_1,t) = \int_0^\infty \frac{1 - \exp((-t/\tau)(R_0/h_1)^6\alpha^6)}{\alpha^3} \, d\alpha \tag{7}$$

and $k = 2/R_0^2$.

In this work, models accounting for liposome aggregation as a result of peptide addition to the lipid suspension were also considered. When two lipid vesicles associate, bilayer adhesion occurs, and an additional plane of acceptors at distance h_2 becomes available for FRET (Figure 1B). The donor decay law is then readily derived from eq 6

$$i_{DA,bilamellar}^{uniform}(t) = i_D(t) \exp[-kC(2h_1^{\,2}F(h_1,t) + h_2^{\,2}F(h_2,t))] \tag{8}$$

If peptide addition induces the formation of a multilamellar structure instead, there are now *two* acceptor planes at distance h_2 from the donor (Figure 1C), and the donor decay law becomes

$$i_{DA,multibilayer}^{uniform}(t) = i_D(t) \exp[-2kC(h_1^{\,2}F(h_1,t) + h_2^{\,2}F(h_2,t))] \tag{9}$$

Note that in the equations above uniform probe distribution is still assumed, together with equal acceptor concentrations in both bilayers.

Another possibility is that the addition of a basic peptide to a binary lipid mixture containing an anionic phospholipid can cause membrane phase separation, leading to a partition of both donor and acceptor probes between the two phases formed. In general, the fluorescence properties of the donor will be different in the two phases as well as the local donor and acceptor concentrations. The overall donor fluorescence intensity decay will be a linear combination of the decays in each phase (which will be given by one of the above equations), weighted by the respective amount of donor molecules present in that phase (proportional to the A factors in the following equation[21])

$$i_{DA}^{phaseseparation}(t) = A_1 i_{DA,phase1}(t) + A_2 i_{DA,phase2}(t) \tag{10}$$

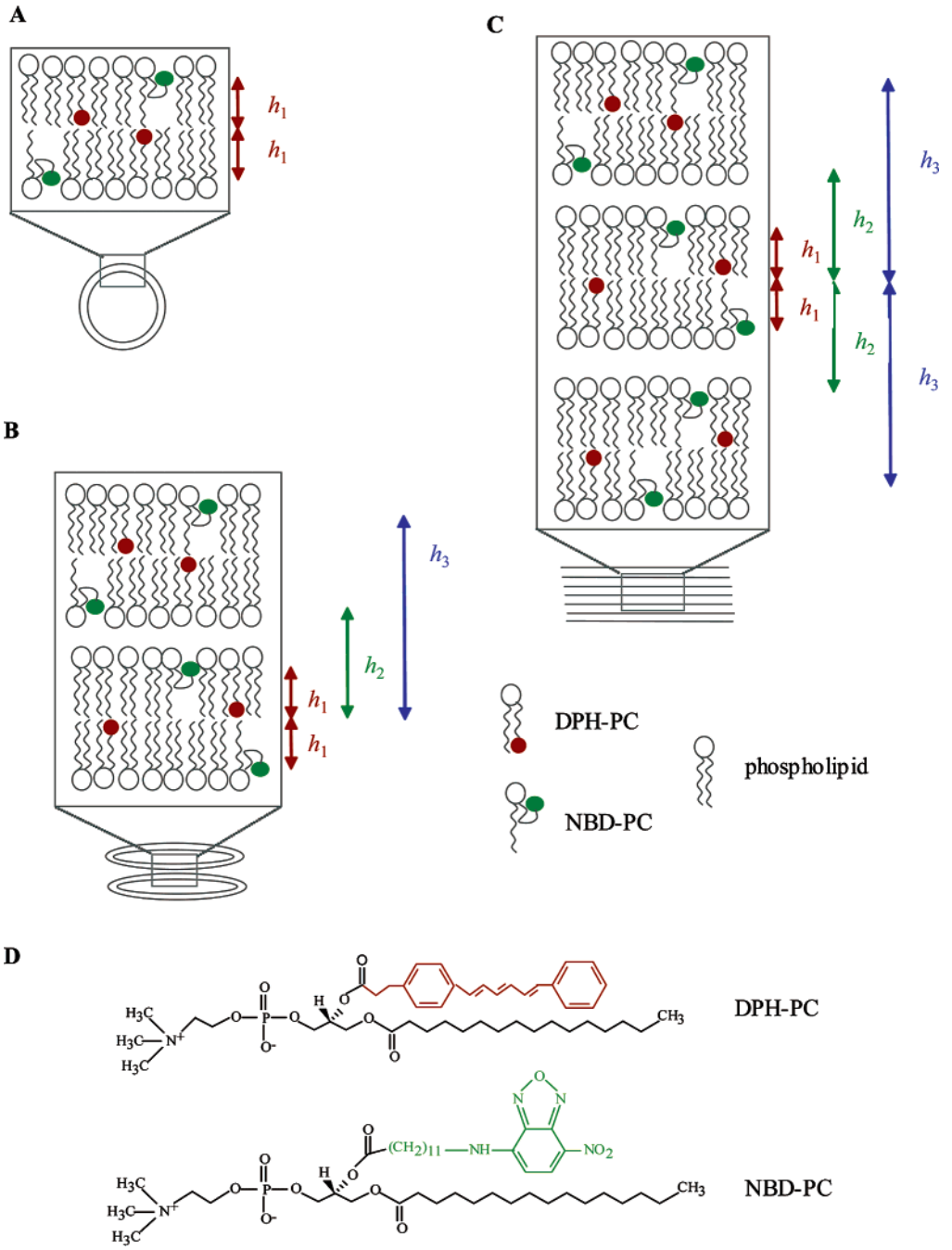

Figure 1. Schematic diagrams of bilayer-based structures considered in the FRET models. (A) Bilayer geometry (eq 6): There are two planes of acceptors (NBD-PC) per donor plane (DPH-PC), both at distance h_1. (B) Bilamellar geometry (eq 8): For each donor plane, there are two acceptor planes at distance h_1 and a single acceptor plane at distance h_2. The additional plane at distance h_3 is neglected in eq 8. (C) Multilayer geometry (eq 9): For each donor plane, there are now two acceptor planes at distances h_1 and h_2, respectively. The two acceptor planes at distance h_3 are also neglected in eq 9. Parts B and C depict situations corresponding to peptide-induced lipid vesicle aggregation driven by electrostatic interactions. The picture is not drawn to scale. (D) Chemical structures of the donor and acceptor probes, DPH-PC and NBD-PC, respectively.

Moreover, if, as often is the case, the donor florescence intensity decay in each phase (in absence of acceptor) is complex, then the above equations can be used, but $i_D(t)$ should be replaced by

$$i_D(t) = \sum_{i=1}^{n} \alpha_i \exp(-t/\tau_i) \tag{11}$$

in eqs 4, 6, 8, 9, and (implicitly) 10, where α_i and τ_i are the amplitude and lifetime of each fluorescence decay component i, respectively. Also, τ should be substituted by the intensity-weighted mean fluorescence lifetime, $\langle\tau\rangle$, in eq 7

$$\langle\tau\rangle = \sum_{i=1}^{n} \alpha_i\tau_i^2 / \sum_{i=1}^{n} \alpha_i\tau_i^2 \tag{12}$$

In all cases, the theoretical FRET efficiency, E_t, is defined by

$$E_t = 1 - \int_0^\infty i_{DA}(t)\,dt / \int_0^\infty i_D(t)\,dt \tag{13}$$

where $i_D(t)$ is the donor decay in the absence of acceptor. The first integral in this equation is calculated numerically.

Materials and Methods

Materials. 1,2-Dipalmitoyl-*sn*-glycero-3-phosphocholine (DPPC), 1,2-dipalmitoyl-*sn*-glycero-3-phosphoserine (DPPS), and 1-palmitoyl-2-[12-(7-nitrobenz-2-oxa-1,3-diazol-4-yl)amino-dodecanoyl]-*sn*-glycero-3-phosphocholine (NBD-PC, Figure 1D) were obtained from Avanti Polar Lipids (Birmingham, AL). 1,3,5-Diphenylhexatriene (DPH) and 1-palmitoyl-2-[3-(diphenylhexatrienyl)propanoyl]-*sn*-glycero-3-phosphocholine (DPH-PC, Figure 1D) were obtained from Molecular Probes (Eugene, OR). The hexalysyltryptophan peptide, K_6W, was purchased from Neosystem (Strasbourg, France). 4-(2-Hydroxyethyl)-1-piperazine sulfonic acid (HEPES), KOH, and KCl (all from Merck, Darmstatdt, Germany) were used to prepare the buffer solution of 10 mM HEPES−KOH (pH 7.4) with 100 mM KCl. All organic solvents were of spectroscopic grade and came from Merck (Darmstatdt, Germany). Deionized water was used throughout. All above materials were used without further purification. The concentrations of stock solutions of peptide and probes were determined spectrophotometrically using the molar absorption coefficient values $\epsilon(K_6W, 280\ nm, in\ buffer) = 5.7 \times 10^3\ M^{-1}\ cm^{-1}$,[27] ϵ(DPH, 350 nm, in CH_3OH) $= 8.8 \times 10^4\ M^{-1}\ cm^{-1}$,[28] ϵ(DPH-PC, 355 nm, in $CHCl_3$) $= 6.0 \times 10^4\ M^{-1}\ cm^{-1}$,[29] and ϵ(NBD-PC, 465 nm, in C_2H_5OH) $= 2.2 \times 10^4\ M^{-1}\ cm^{-1}$.[28]

Lipid Vesicle Preparation. Large unilamellar vesicles (LUVs, ∼100 nm in diameter), containing the desired molar ratio of DPPC and DPPS, were prepared by extrusion of lipid dispersions through 100-nm-pore-diameter polycarbonate membranes as previously described.[30] The resulting lipid dispersions were stored at room temperature and used within 24 h of preparation. The concentrations of phospholipid stock solutions were determined using phosphate analysis.[31]

Instrumentation. Absorption spectroscopy was carried out with a Jasco V-560 spectrophotometer. When necessary, absorption spectra were corrected for turbidity using the method of Castanho et al.[32] Steady-state fluorescence measurements were carried out with an SLM-Aminco 8100 series 2 spectrofluorimeter in a right-angle geometry with the cell holder thermostated at the required temperature (±0.05 °C) using a circulating water bath. The light source was a 450 W Xe arc lamp, and the reference was a rhodamine B quantum counter solution. Correction of emission spectra was performed using the correction software of the apparatus. The 5 mm × 5 mm quartz cuvettes were used throughout.

The steady-state fluorescence anisotropy, $\langle r \rangle$, was measured using Glan-Thompson polarizers

$$\langle r \rangle = \frac{I_{VV} - GI_{VH}}{I_{VV} + 2GI_{VH}} \tag{14}$$

The different intensities I_{ij} in eq 14 are the steady-state vertical and horizontal components of the fluorescence emission with excitation vertical (I_{VV} and I_{VH}, respectively) and horizontal (I_{HV} and I_{HH}, respectively) to the emission axis. The latter pair of components is used to calculate the G factor ($G = I_{HV}/I_{HH}$).[33] An adequate blank was subtracted from each intensity reading before calculating the anisotropy value.

Fluorescence decay measurements were carried out with a time-correlated single-photon counting system, which is described elsewhere.[34] Excitation and emission wavelengths were 288 and 345 nm (respectively) for K_6W, 335 and 430 nm (respectively) for DPH-PC, and 332 and 533 nm (respectively) for NBD-PC. Time scales were chosen for each sample to observe the decay through 2−3 intensity decades. Instrumental response functions for deconvolution were generated from a scattering dispersion (silica, colloidal water suspension, Aldrich, Milwaukee, WI). Data analysis was carried out using a nonlinear least-squares iterative convolution method based on the Marquardt algorithm. The goodness of the fits was judged from the experimental χ^2 values, weighted residuals, and autocorrelation plots.

Membrane/Water Partition Coefficient Measurements of the Peptide K_6W. The partitioning of K_6W into the mixed lipid vesicles of 50:50 DPPC/DPPS was determined by performing time-resolved fluorescence measurements of the peptide. Briefly, after incubation of the samples for 1 h at the desired temperature, the fluorescence emission decay kinetics of the peptide (1.7 μM final concentration) was measured as a function of the lipid concentration of the samples at $T = 45$ °C and $T = 60$ °C. The tryptophan residue of the peptide was excited at 287 nm, and its fluorescence emission was detected at 345 nm. The lifetime-weighted quantum yields, $\bar{\tau}$, were calculated from the fluorescence intensity decays (eq 11) according to[33]

$$\bar{\tau} = \sum_{i=1}^{3} \alpha_i \tau_i \tag{15}$$

The partitioning experiments were then analyzed using[35]

$$\bar{\tau} = \bar{\tau}_W + \frac{(\bar{\tau}_L - \bar{\tau}_W) K_p [L]_{ac}}{[W] + K_p [L]_{ac}} \tag{16}$$

In this equation, $\bar{\tau}_i$ is the lifetime-weighted quantum yield in phase i (i = L or W, for lipid and aqueous phases, respectively), K_p is the membrane/water partition coefficient of the peptide, $[W]$ is the molar concentration of water, and $[L]$ is the molar concentration of lipid. It was assumed that only 50% of the overall lipid used was available for the binding of the externally added peptide, $[L]_{ac}$.

Gel/Fluid Partition Coefficient Measurements of the Lipid Probes. When the lipid mixture under study undergoes phase separation, the fluorescently labeled phospholipid distributes between the two phases i (i = G or F, for gel and fluid phases, respectively), and the molar fraction of the probe in phase i, P_i, depends on the amount of each phase (molar fraction X_i) and on its gel/fluid partition coefficient, $K_p^{g/f}$, according to[36]

$$K_p^{g/f} = (P_G/X_G)/(P_F/X_F) \tag{17}$$

Two different fluorescence methodologies were used in this work to measure the distribution of the donor and acceptor probes between the gel and fluid phases. For DPH-PC (donor), its steady-state fluorescence anisotropy, $\langle r \rangle$, was measured as a function of the molar fraction of the gel phase, X_G, present in the different DPPC/DPPS lipid mixtures prepared[37]

$$\langle r \rangle = \frac{K_p^{g/f} X_G \bar{\tau}_G \langle r \rangle_G + (1 - X_G) \bar{\tau}_F \langle r \rangle_F}{K_p^{g/f} X_G \bar{\tau}_G + (1 - X_G) \bar{\tau}_F} \tag{18}$$

The excitation and emission wavelengths used for DPH-PC were 360 and 431 nm, respectively, and 2 nm slits were used in these measurements. For NBD-PC (acceptor), the dependence of its lifetime-weighted quantum yield, $\bar{\tau}$, on the variable molar fraction of the gel phase, X_G, present in the different DPPC/

DPPS lipid mixtures prepared was determined[37]

$$\bar{\tau} = \frac{K_p^{g/f} X_G \bar{\tau}_G + (1 - X_G)\bar{\tau}_F}{K_p^{g/f} X_G + (1 - X_G)} \quad (19)$$

The excitation and emission wavelengths used for NBD-PC were 332 and 533 nm, respectively. In both cases, $K_p^{g/f}$ was the only parameter allowed to vary during the least-squares analysis performed on the experimental data of either $\langle r \rangle$ versus X_G[37] (eq 18) or $\bar{\tau}$ versus X_G[37] (eq 19). Both the donor, DPH-PC, and the acceptor, NBD-PC, probes were cosolubilized with the phospholipid mixtures to obtain final probe/lipid ratios of 1:500. The molar fractions of each phase present in the DPPC/DPPS lipid mixtures studied at 45 °C were computed using the lever rule and assuming that the extremes of the tie-line at this temperature corresponded to 75:25 and 20:80 DPPC/DPPS, respectively.

FRET Measurements. The energy transfer experiments between DPH-PC (donor) and NBD-PC (acceptor) were carried out in 50:50 DPPC/DPPS LUVs, at both $T = 45$ °C and $T = 60$ °C. The probe/lipid ratios used were 1:1000 and 1:250 for the donor and the acceptor, respectively. After incubation of the samples prepared only with donor, D, and with donor and acceptor, D + A, for 1 h at the adequate temperature, increasing concentrations of K_6W were added to different lipid suspensions from a ca. 300 μM peptide stock solution in the standard buffer (final peptide concentrations between 0 and 150 μM; final lipid concentration of 0.75 mM). As a control, the effect of adding 150 μM peptide to an acceptor-only lipid sample was also studied. Then, the fluorescence intensity decays of the donors were measured subsequently to an additional incubation period of 1 h at the required temperature for all the samples. After empirical analysis of the decays using a sum of exponentials (eq 11), the experimental efficiency of energy transfer was calculated as

$$E_{exp} = 1 - \bar{\tau}_{DA}/\bar{\tau}_D \quad (20)$$

Here, $\bar{\tau}_{DA}$ and $\bar{\tau}_D$ are the lifetime-weighted quantum yields of the donor in the presence and in the absence of acceptor, respectively. The excitation wavelength was 340 nm for all of the samples, and the emission wavelengths were 430 and 540 nm for the donor and the acceptor, respectively.

R_0 is the distance at which the transfer efficiency is 50% for an isolated donor−acceptor pair and was calculated using eq 2. For this purpose, the quantum yield of the donor, Φ_D, was determined for DPH-PC at an excitation wavelength of 355 nm, relative to a standard of quinine sulfate in 0.1 N H_2SO_4 (Φ_r = is 0.546 in 0.1 N H_2SO_4[38]), using polarizers oriented at the magic angle.

Results

Characterization of the System. The temperature/composition phase diagram of the binary lipid mixture DPPC/DPPS previously determined by Luna and McConnell[39] was first confirmed by measuring the steady-state fluorescence anisotropy of DPH as a function of temperature at different DPPC/DPPS molar ratios (data not shown). From this diagram, the temperatures chosen to perform the FRET studies were 45 and 60 °C because in the first case the equimolar DPPC/DPPS mixture exhibits gel/fluid coexistence, with similar amounts of gel and fluid phases, and at 60 °C it is well above T_m(DPPS), and so the entire membrane is in the fluid phase.

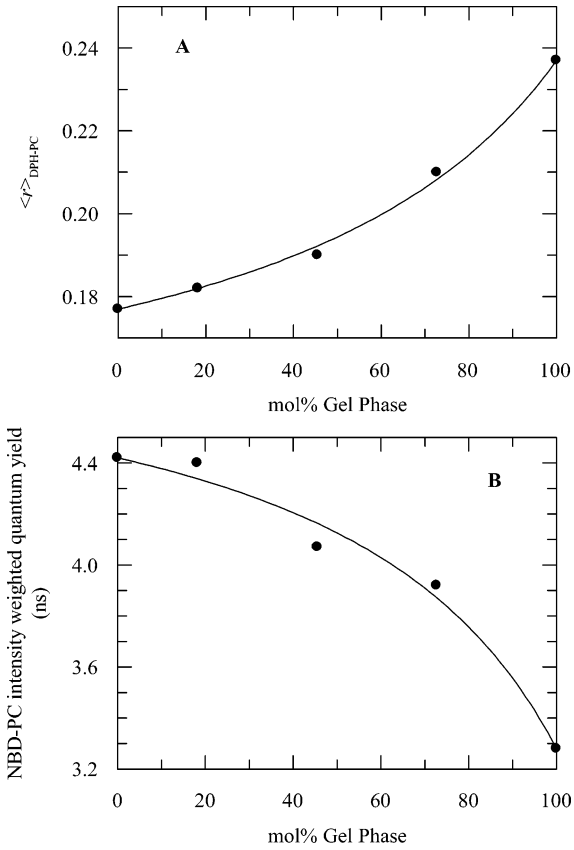

Figure 2. (A) Steady-state fluorescence anisotropy of DPH-PC (donor, 0.2 mol %) ($\lambda_{exc} = 360$ nm; $\lambda_{em} = 431$ nm) and (B) lifetime-weighted quantum yield of NBD-PC (acceptor, 0.2 mol %) ($\lambda_{exc} = 332$ nm; $\lambda_{em} = 533$ nm) in DPPC/DPPS 1 mM LUVs at $T = 45$ °C as a function of the mol % of gel phase. The lines are the best fits of eqs 16 and 18 to the experimental data with $K_p^{g/f}$ (DPH-PC) = 0.32 ± 0.02 and $K_p^{g/f}$ (NBD-PC) = 0.31 ± 0.06, respectively.

The fluorescence intensity decays of K_6W were measured in both the presence and the absence of DPPC/DPPS equimolar mixtures at both temperatures. All samples had complex decays, and a sum of three exponentials was required to describe them adequately. For both temperatures, the lifetime-weighted quantum yield of the peptide increased hyperbolically with the available lipid concentration, indicating peptide partition to the bilayer, and $K_p = (4.1 \pm 1.8) \times 10^5$ ($T = 45$ °C) and $K_p = (5.5 \pm 1.7) \times 10^5$ ($T = 60$ °C) were obtained from fitting eq 16 to the experimental data (data not shown).

The chosen phospholipid probes, DPH-PC and NBD-PC (Figure 1D), were both expected a priori to prefer the fluid phase (richer in DPPC) relative to the gel phase (richer in DPPS) for DPPC/DPPS mixtures inside the phase coexistence range due to their headgroups. To confirm this result, their gel/fluid partition coefficients ($K_p^{g/f}$, eq 17) were determined at $T = 45$ °C. Whereas the fluorescence intensity or lifetime of DPH-PC in DPPC/DPPS mixtures is almost insensitive to the lipid composition used (data not shown), $\langle r \rangle$ increases steadily upon increasing the gel phase fraction (X_G), as shown in Figure 2A. This variation was used to calculate $K_p^{g/f} = 0.32 \pm 0.02$ for this probe by fitting eq 18 to the measured $\langle r \rangle$ values. In this fit, the only parameter allowed to vary was $K_p^{g/f}$, whereas $\bar{\tau}_G = 7.04$ ns, $\bar{\tau}_F = 6.72$ ns, $\langle r \rangle_G = 0.237$, and $\langle r \rangle_F = 0.177$ were fixed during the least-squares analysis.

For NBD-PC, the variation of $\langle r \rangle$ versus X_G was much smaller than that of $\bar{\tau}$ (data not shown), and this latter parameter was used to obtain $K_p^{g/f} = 0.31 \pm 0.06$ for this probe by fitting eq

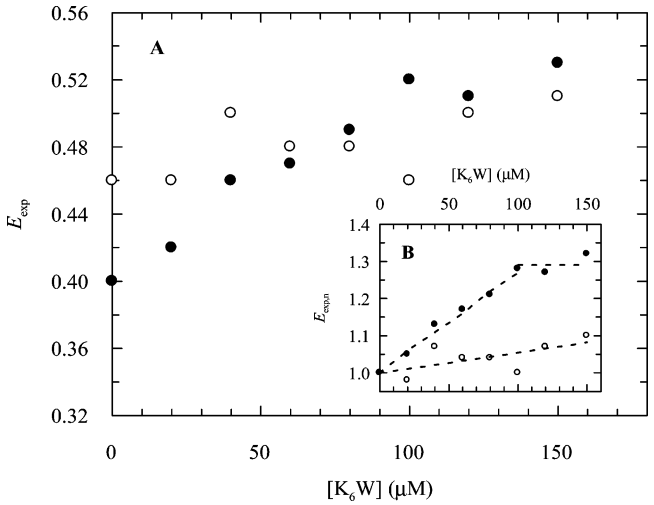

Figure 3. (A) Variation of the experimental FRET efficiency, E_{exp}, with the peptide concentration, [K$_6$W], for DPH-PC (0.1 mol %)/NBD-PC (0.4 mol %) donor/acceptor pair in 50:50 DPPC/DPPS 0.75 mM LUVs (T = 45 °C (○) and T = 60 °C (●)). (B) Experimental FRET efficiencies normalized to the value obtained in absence of the peptide. The lines are drawn to guide the eye.

19 to the experimental $\bar{\tau}$ values (Figure 2B). Again, $\bar{\tau}_G$ = 3.28 ns and $\bar{\tau}_F$ = 4.42 ns were preset, and $K_p^{g/f}$ was the only parameter varied in the fit. The values obtained for the gel/fluid partition coefficients of the probes, $K_p^{g/f} < 1$, confirm that both probes prefer the fluid phase at this temperature.

FRET Experiments. The emission spectrum of DPH-PC overlaps significantly the absorption spectrum of NBD-PC, and therefore DPH-PC can be used as a FRET donor to NBD-PC. The Förster radii for this pair were calculated to be 40.5 and 39.8 Å at T = 45 °C and T = 60 °C, respectively, using the measured spectra in eq 3, together with n = 1.4,[21] $\kappa^2 = {}^2/_3$ (dynamic isotropic limit value), and the measured quantum yields Φ_D (T = 45 °C) = 0.56 and Φ_D (T = 60 °C) = 0.51, respectively.

The influence of K$_6$W on the distribution of the fluorescently labelled phospholipids on the lipid vesicles was evaluated by performing time-resolved fluorescence measurements of the donor, in the absence and in the presence of acceptors, at different final peptide concentrations. As a control, it was found that the fluorescence emission decays of both the donor, DPH-PC, and the acceptor, NBD-PC, were not affected by the addition of the peptide even at the highest concentration used (150 μM, data not shown), precluding that K$_6$W directly quenched the donor/acceptor fluorescence.

The experimental FRET efficiencies for each peptide concentration were computed with eq 20 using the time-resolved data. Figure 3A shows that the energy transfer efficiencies between DPH-PC and NBD-PC in DPPC/DPPS 50:50 already show large values in the absence of K$_6$W for both T = 45 °C ($E_{exp} \approx 0.46$) and T = 60 °C ($E_{exp} \approx 0.40$). The value obtained for this parameter at the highest temperature used is close to E_t = 0.43, the theoretical expectation for a uniform distribution of acceptors in a trans geometry relative to the donor (computed from eqs 6, 7, and 13). In this calculation, the vertical separation distance between a donor−acceptor pair was considered to be h_1 = 17 Å (corresponding to half of the bilayer width[40]) because, whereas it is a good approximation to admit that the DPH moiety of DPH-PC is located in the center of the bilayer, the fluorophore group of NBD-PC is known to snorkel to the bilayer interface.[41] In addition, a lateral area per phospholipid molecule of 71 Å^2 was used (this is the value reported as for DPPC at T = 50 °C[40]) when calculating the surface density of acceptors.

TABLE 1: Parameters Obtained from Pairwise Global Analysis of the Time-Resolved Decays of DPH-PC (Donor) in the Absence and in the Presence of NBD-PC (Acceptor) for Equimolar DPPC/DPPS 50:50 LUVs at Different Peptide Concentrations (T = 45 °C)

	model						
	uniform distribution, trans geometry (eq 6)[a]		phase separation, trans geometry (eq 10)[b]				
[K$_6$W] (μM)	C	χ_g^2	C_1	C_2	$K_{PD}^{g/f}$ [c]	$K_{PA}^{g/f}$ [d]	χ_g^2
0	0.457	2.13	0.000	0.705	0.24	0	1.43
20	0.411	2.22	0.000	0.761	0.33	0	1.23
40	0.494	2.01	0.023	0.758	0.22	0.042	1.31
60	0.457	2.10	0.157	0.936	0.49	0.23	1.20
80	0.537	1.80	0.081	0.748	0.19	0.15	1.39
100	0.463	2.22	0.149	0.941	0.55	0.22	1.27
120	0.495	1.99	0.223	0.936	0.64	0.32	1.28
150	0.509	1.93	0.132	0.835	0.34	0.22	1.18

[a] h_1 = 17 Å was used. [b] h_1 = 22 Å and h_2 = 17 Å were used. [c] Calculated using $K_{PD}^{g/f} = (A_G/X_G)/(A_F/(1 - X_G)) = (A_1/X_G)/(A_2/(1 - X_G))$. X_G = 0.454 was taken from the measured phase diagram (data not shown). [d] Calculated using $K_{PA}^{g/f} = (C_G a_G)/(C_F a_F) = (C_1 a_1)/(C_2 a_2)$, where a_i is the area/phospholipid in the bilayer plane in phase i (a_G = 52 Å^2 and a_F = 71 Å^2 were used).

At 60 °C, when K$_6$W was added to the lipid suspensions, E_{exp} increased up to ∼0.53 (at a final peptide/lipid ratio of 1:5, Figure 3A), a result compatible with a peptide-induced lateral phase separation and/or membrane aggregation. This increase is especially steep at lower peptide concentrations (<100 μM), as visible in Figure 3B (where FRET efficiencies are normalized respective to the value obtained in absence of peptide). The observation of a plateau for [K$_6$W] ≅ 100 mM suggests that the cationic peptide can bind a maximum of 2−3 anionic phospholipids (if one admits that only 50% of total DPPS is available for complex formation), which is in fair agreement with the tetralysine and pentalysine binding stoichiometries of 2.4−2.5 and 2.0−2.6, respectively, determined for 1,2-dipalmitoyl-*sn*-glycero-3-[phosphor-rac-(1-glycerol)] by Kleinschmidt and Marsh[42] in an electron spin resonance spectroscopy study. However, the addition of peptide to the gel/fluid mixture (T = 45 °C) did not lead to a significant increase of the experimental FRET efficency (E_{exp} = 0.48 ± 0.02, Figure 3A); i.e., it seems that there was no detectable rearrangement of the preexisting lipid domains.

Additionally, the time-resolved donor fluorescence decay curves were analyzed using the formalisms described in the FRET Theoretical Background section. The data obtained at 45 °C (Table 1) and 60 °C (Table 2) were both analyzed using the uniform distribution, bilayer geometry model (eq 6, with h_1 fixed at 17 Å) and the phase separation, bilayer geometry model (eq 8, with fixed $h_1 = h_G$ = 22 Å and $h_2 = h_F$ = 17 Å, the values expected for half-bilayer widths for palmitoyl chains in the gel and fluid phases, respectively[40]). In the latter analysis, the donor decay was assumed to be identical in the gel and fluid phases. This simplification is justified because the DPH-PC lifetime-weighted quantum yield is almost invariant in the whole composition range at T = 45 °C, from pure DPPC ($\bar{\tau}$ = 7.0 ns) to pure DPPS ($\bar{\tau}$ = 7.3 ns) at the same temperature. Furthermore, the data obtained at the higher temperature were also analyzed using the uniform distribution, bilamellar geometry model (eq 8) and the uniform distribution, multilamellar geometry model (eq 9). In the latter two cases, h_1 was fixed at 17 Å, whereas the distance to the second plane of acceptors,

TABLE 2: Parameters Obtained from Pairwise Global Analysis of the Time-Resolved Decays of DPH-PC (Donor) in the Absence and in the Presence of NBD-PC (Acceptor) for Equimolar DPPC/DPPS 50:50 LUVs at Different Peptide Concentrations ($T = 60$ °C)

	model									
	uniform distribution, trans geometry (eq 6)[a]		phase separation, trans geometry (eq 10)[b]		uniform distribution, bilamellar geometry (eq 8)[c]			uniform distribution, multi-bilayer geometry (eq 9)[c]		
[K_6W] (μM)	C	χ_g^2	$C_1 = C_2$	χ_g^2	C	h_2 (Å)	χ_g^2	C	h_2 (Å)	χ_g^2
0	0.395	1.25	0.395	1.25	0.355	54	1.22	0.359	67	1.22
20	0.441	1.61	0.441	1.61	0.323	35	1.26	0.376	58	1.33
40	0.515	1.59	0.515	1.59	0.415	43	1.28	0.433	57	1.29
60	0.537	1.39	0.535[d]	1.24	0.417	40	0.98	0.438	54	0.99
80	0.582	2.34	0.584	2.34	0.448	39	1.37	0.411	45	1.30
100	0.677	4.23	0.677	4.23	0.525	39	1.99	0.448	41	1.29
120	0.688	4.98	0.688	4.98	0.531	38	2.34	0.450	40	1.35
150	0.739	5.87	0.739	5.87	0.572	38	2.63	0.486	40	1.39

[a] $h_1 = 17$ Å was used. [b] $h_1 = 22$ Å and $h_2 = 17$ Å were used. [c] $h_1 = 17$ Å was used. [d] $C_1 = 0.553$, $C_2 = 0.522$.

h_2, was optimized in each fit. A detailed discussion of these analyses will be presented in the next section.

Discussion

In this work, we studied the interaction of a model cationic peptide (K_6W) with membranes composed of one anionic (DPPS) and one zwitterionic (DPPC) phospholipid, in both one-phase (fluid, $T = 60$ °C) and two-phase (gel/fluid, $T = 45$ °C) conditions. The spectral properties of the peptide showed virtually no differences in the absence and in the presence of LUVs (result not shown), indicating that the tryptophan residue remains exposed to the aqueous phase.[43] However, its lifetime-weighted quantum yield increased upon increasing the phospholipid concentration, allowing the use of this parameter to characterize the peptide partition between lipid vesicles and buffer. The values obtained, $K_p = (4.1 \pm 1.8) \times 10^5$ and $K_p = (5.5 \pm 1.7) \times 10^5$ for $T = 45$ °C and $T = 60$ °C, respectively, reveal little sensitivity to temperature. This effect was already described for other polylysine peptides,[44] suggesting that the change in enthalpy upon peptide binding is small, which is characteristic of electrostatic interaction.[45−47]

Molecular Topological and Topographical Changes Caused by a Basic Peptide on Two-Component Lipid Vesicles Analyzed by FRET. Due to the strong distance dependence (eq 1) of the FRET interaction, FRET measurements are expected to be sensitive to a redistribution of the membrane probes in the lipid bilayer and/or to liposome aggregation caused by an external factor (peptide addition), eventually reporting the formation of lipid domains and/or stacking of the lipid membranes. Because both DPH-PC and NBD-PC prefer the fluid, DPPC-rich phase in the gel/fluid coexistence range (as expected beforehand and verified experimentally; see Figure 2), if peptide addition to the vesicles induced a lateral segregation of the anionic phospholipids, then the surface concentration of acceptors (in the remaining DPPC-enriched phase) would necessarily increase, and the efficiency of energy transfer would be expected to increase concomitantly. A similar effect upon E could potentially result from the distinct phenomenon of peptide-induced vesicle aggregation, because this process would produce additional planes of acceptors within quenching distance of each donor (Figures 1B and 1C).

As a first approach in data analysis, fluorescence intensity decays were described by empirical sum-of-exponentials functions, and the recovered fitting parameters were used to calculate the experimental FRET efficiencies, E_{exp}, using eq 20 (Figure 3). At $T = 60$ °C and for peptide-free vesicles, there was a fair agreement between the experimental and the theoretical value calculated for a uniform distribution of acceptors (see above). When K_6W was added to the lipid vesicles, E_{exp} increased up to 0.54 (for a peptide/lipid ratio of 1:5), whereas addition of peptide to the gel/fluid mixture ($T = 45$ °C) did not lead to a significant increase in E_{exp}.

However, despite being a rapid way of obtaining a first glimpse into the possible membrane organization, the steady-state analysis information is always limited. The FRET efficiency parameter results from time integration of the actual decay law, and in this process considerable detail regarding the probe distribution is lost. Thus, whenever possible, a complete parameter analysis of the time-resolved fluorescence donor decays should be carried out (ideally with pairwise global analysis of samples with and without acceptor), as reviewed recently.[21]

Time-Resolved FRET Analysis: Gel/Fluid Coexistence Region. In this study, analysis of the fluorescence decays recorded at 45 °C was first attempted with the FRET formalism corresponding to a uniform distribution of probes with a trans geometry (eq 6, together with eqs 5 and 7, and assuming $h_1 = 17$ Å). As shown in Table 1, unacceptable large values of the global chi-square ($\chi_g^2 > 1.8$) were recovered for all K_6W concentrations studied (including [K_6W] = 0 μM). This was expected because in the absence of peptide there is already phase separation in the lipid bilayers. The logical step in this situation was then to analyze the decays using the phase separation formalism, again considering a trans geometry (eq 10). This type of situation has been previously observed in systems bearing gel/fluid[37] and liquid ordered/liquid disordered phase separation.[48,49] In accordance, the pairwise analysis of the donor fluorescence decays with the phase separation formalism was successful ($\chi_g^2 < 1.5$ for all samples, Table 1).

For all samples, the phase with the larger recovered C component (which is proportional to the surface density of acceptors, eq 5) in the FRET decay (C_2 in Table 1) was consistently associated with the larger recovered A value in eq 10 ($A_2/A_1 > 1$ for all systems in Table 1, data not shown) and $h_2 = h_F = 17$ Å. This is the fluid phase, in which both the acceptor concentration and amount of donor are larger. The recovered parameters allow the estimation of the partition coefficients of both the donor and the acceptor probes for each peptide concentration, as demonstrated elsewhere.[37] For the acceptor (assuming identical donor decays in the two phases), $K_{PA}^{g/f} = (C_G a_G)/(C_F a_F) = (C_1 a_1)/(C_2 a_2)$, where a_i is the area per phospholipid in the bilayer plane in phase i (i = G or F for the fluid and gel phases, respectively). The values in Table 1 were obtained using the typical values $a_G = 52$ Å^2 and $a_F = 71$ Å^2.[40]

For the donor, $K_{PD}^{g/f} = (A_G/X_G)/(A_F/X_F) = (A_1/X_G)/(A_2/X_F)$. X_G and $X_F = 1 - X_G$ are obtained from the relevant composition and temperature values from the measured phase diagram, using the lever rule (for the equimolar composition at 45 °C, $X_G = 0.454$ is obtained (data not shown)). One can compare cautiously these $K_p^{g/f}$ values (Table 1) with those obtained from independent experiments (variations of $\langle r \rangle$ (Figure 2A) and $\bar{\tau}$ (Figure 2B) with the lipid compositions of the vesicles for the donor and acceptor, respectively) in the absence of peptide. Qualitatively, these FRET and non-FRET partition coefficient values agree in that they all point to probe preference for the fluid phase. Quantitative differences (for example, the zero $K_{PA}^{g/f}$ value obtained from the FRET analysis parameters) are justified bearing in mind (i) the approximations commented above in the FRET analysis, (ii) the fact that the FRET values were obtained from a single point in the tie-line, instead of a fit to several data points, and (iii) possible uncertainty regarding the best R_0 value for the gel phase, which could stem from incomplete sampling of donor−acceptor relative orientation during the donor excited-state lifetime. Addition of peptide does not lead to significant change in probe partition, and a nonmonotonic variation is observed for both gel/fluid partition coefficients of the donor ($K_{PD}^{g/f} = 0.38 \pm 0.17$, $n = 8$) and acceptor ($K_{PA}^{g/f} = 0.20 \pm 0.09$, $n = 6$), respectively. The $K_{PD}^{g/f}$ value calculated in this way agrees in fact fairly well with the value calculated from $\langle r \rangle_{DPH-PC}$ variation ($K_p^{g/f} = 0.32 \pm 0.02$). The recovery of a smaller value for $K_{PA}^{g/f}$ in the FRET calculation probably stems from the discussed approximations, which should also be related to the large relative fluctuations in the small (and more difficult to recover accurately) gel C value (C_1) but smaller relative fluctuations in the large (fluid) C value (C_2). The fact that the FRET $K_{PA}^{g/f}$ value is not closer to unity than that measured using the variation of $\bar{\tau}$ ($K_p^{g/f} = 0.31 \pm 0.06$, Figure 2B) indicates that the coexisting phases form domains that are large in the FRET scale (probably larger than $\sim 5R_0 = 200$ Å[48]) for all peptide concentrations used. The lack of significant and systematic variation of any of the recovered parameters points to the inability of the peptide to change appreciably the domain organization in this system, confirming the FRET efficiency invariance shown in Figure 3.

Time-Resolved FRET Analysis: Fluid Phase. For $T = 60$ °C, data analysis (Table 2) gave results that are strikingly different from those obtained for $T = 45$ °C in a number of ways. First, the uniform distribution model/trans geometry (eq 5) yields a satisfactory fit in the absence of peptide. The recovered C parameter agrees well with the value expected from eq 6 ($C = 0.379$). This indicates that the probe distribution at this temperature is indeed uniform, and there is no phase separation or microheterogeneity for this mixture, even in the FRET length scale. This is not a trivial result, and indeed there are examples in the literature of FRET measurements in other phospholipid mixtures above the main transition temperatures of both components that showed disagreement between expected (for uniform distribution of probes) and observed FRET efficiencies (e.g., 1,2-dilauroyl-*sn*-glycero-3-phosphocholine/1,2-stearoyl-*sn*-glycero-3-phosphocholine at $T = 65$ °C[50]). However, upon addition of peptide, the FRET decays could no longer be analyzed assuming a uniform distribution of probes with a trans geometry in a bilayer, as the goodness of fit steadily decreases. Even for the lowest nonzero peptide concentration used, the χ_g^2 value is already unacceptable. The recovered C value in these poor fits is considerably higher than that for $[K_6W] = 0$ μM, seeming to indicate higher acceptor average local concentrations around the donors. This was already hinted from the increase in FRET efficiency mentioned above (Figure 3). This clearly shows that the peptide alters the membrane organization and made us consider the possibility of phase separation again associated with a trans geometry (eq 10). However, this new analysis failed to increase the quality of the fits (Table 2), and even if distinct values of C_1 and C_2 were used as initial approximations, the iterative fitting procedure slowly converged to $C_1 = C_2 =$ recovered C in the previous uniform distribution model/trans geometry analysis.

The inability of the phase separation model to describe the measured decays stems from their shape. Figure 4A compares the fluorescence decays of the donor in the absence of acceptor (curve a, $[K_6W] = 0$ μM), in the presence of acceptor for $[K_6W] = 0$ μM (curve b), and for $[K_6W] = 150$ μM (curve c). The decays for the samples with acceptor are faster than that for the sample without acceptor, as a consequence of the FRET interaction. However, curves b and c have very different shapes, even though the bulk concentration of the acceptor probe is the same in both. The decay for $[K_6W] = 0$ μM (curve b) shows the typical profile for a two-dimensional or quasi-two-dimensional geometry (bilayer). For short times, the decay is very fast. At longer times it slows down, and ultimately (for $t > 15$ ns in Figure 4A) it becomes almost parallel (in a semilog plot) to that in the absence of acceptor. For $[K_6W] = 150$ μM (Figure 4A, curve c), after an initial ($t < 2$ ns) regime similar to that obtained with $[K_6W] = 0$ μM, the decay takes much longer than for curve b to become parallel to that in the absence of acceptor. Therefore, addition of peptide from $[K_6W] = 0-150$ μM gradually transformed the donor decay in the presence of acceptor from curve b to curve c and rendered it impossible to analyze with eq 6 or 10. This prompted us to consider the occurrence of a FRET component to planes of acceptors characterized by a higher h_1 value for $[K_6W] > 0$ μM. In this situation, the decay curve slope (in semilog plots) returns to that of the donor alone more slowly. However, this cannot be realized simply by an increase of h_1 (or, in physical terms, by an increase of bilayer width, which could result from some hypothetical ordering of the acyl chains by the peptide) because in those circumstances (i) the decay should still be analyzed successfully using eq 6 with an increased h_1 value and (ii) it would actually be slower than that for $[K_6W] = 0$ μM, which is not verified. However, if there were two FRET components, one to a closer plane of acceptors ($h_1 = 17$ Å) and an *additional* one to a further plane of acceptors at a distance h_2, then the decay would now be faster than that for $[K_6W] = 0$ μM (and FRET efficiency would concomitantly be larger, as observed in Figure 3). Additional planes of acceptors could arise from two distinct arrangements, as described in the FRET Theoretical Background section and schematically depicted in Figure 1. The aggregation of only two lipid vesicles (Figure 1B) leads to eq 8 for the donor decay (the number of acceptors at distance h_2 is half of that at distance h_1), whereas formation of a multilamellar structure, with stacked bilayers (Figure 1C), leads to eq 9 instead (the number of acceptors at distance h_2 is equal to that at distance h_1).

In this context, global analyses of the time-resolved data were again attempted with both eqs 8 and 9 (in each case, by fixing $h_1 = 17$ Å and optimizing h_2) to find out if any of the underlying models adequately fitted the experimental data. For $T = 45$ °C, the data could not be analyzed with either of these equations (the deconvolution software did not converge). However, for $T = 60$ °C and $[K_6W] < 100$ μM, both models produced acceptable fits as shown in Table 2. In this peptide concentration range, there is a general trend of C increasing and h_2 decreasing

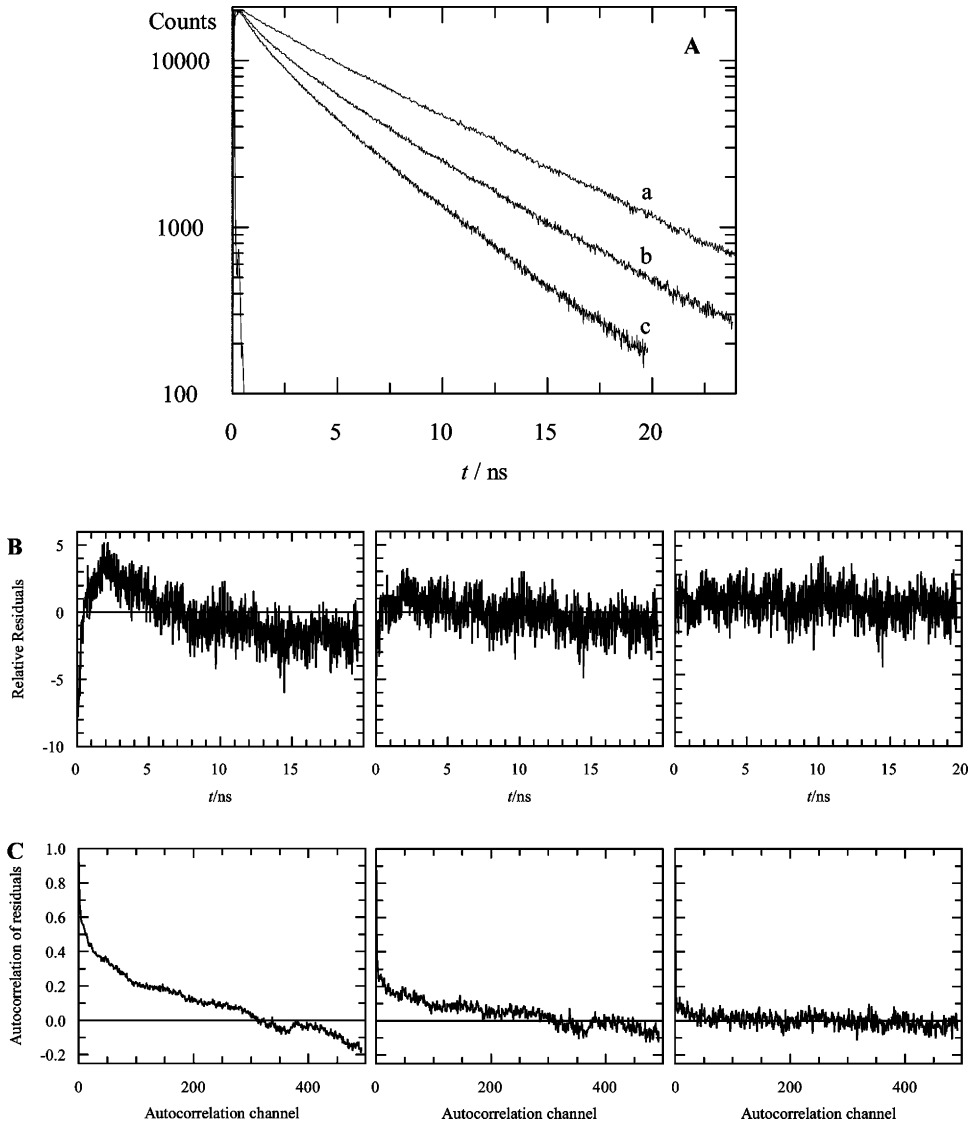

Figure 4. (A) Fluorescence decays of DPH-PC in 50:50 DPPC/DPPS 0.75 mM LUVs at 60 °C: (a) no acceptor, $[K_6W] = 0$ μM; (b) NBD-PC, total lipid = 1:250, $[K_6W] = 0$ μM; (c) NBD-PC, total lipid = 1:250, $[K_6W] = 150$ μM. The excitation profile is also shown. (B) Residuals and (C) autocorrelation of residuals of the fits to the fluorescence decay of DPH-PC: NBD-PC, total lipid = 1:250, $[K_6W] = 100$ μM. The models used were, from left to right, in both panels: trans geometry (eq 6), bilamellar geometry (eq 8), and multi-bilayer geometry (eq 9).

with increasing $[K_6W]$ for both models. Only the parameters recovered from the two-aggregated-lipid-vesicles (bilamellar) model analysis of $[K_6W] = 20$ μM seem to be off this trend. This is probably due to a rather shallow χ_g^2 hypersurface, as, for example, ($h_2 = 43$ Å, $C = 0.367$) led to $\chi_g^2 = 1.29$ (still acceptable and better than any other model, but now within the trend formed by the other results). This result underlines the need to take into account the general trend obtained from several samples, rather than just a single one, when discussing analyses with these complex models. In any case, note that there are only three fitting parameters for each donor−acceptor sample (all lifetimes and preexponential ratios are linked to—and markedly restricted by—the corresponding donor decay, leaving h_2, C, and a sole preexponential as the only nonlinked parameters) in both models, and the $[K_6W] = 20$ μM data analysis with eq 8 is the only off-trend result. We therefore believe that the χ_g^2 variations presented in Table 2 are, on the whole, significant. In the range $[K_6W] < 80$ μM, the two-aggregated-lipid-vesicles (bilamellar) model (eq 8) yielded slightly better statistics, with generally higher C and lower h_2 values (compensating for the loss of one acceptor plane at distance h_2) than the multi-bilayer model (eq 9). This is reversed for $[K_6W] = 80$ μM, for which the lower χ_g^2 is obtained with the multilamellar model. For this peptide concentration, the bilamellar fit is still acceptable ($\chi_g^2 < 1.5$), but this is no longer the case for higher peptide concentrations. Already for $[K_6W] = 100$ μM, a clear improvement in the quality of fitting with the multilamellar model is observed in the residuals' and autocorrelation of residuals' plots shown in Figures 4B and 4C. For $[K_6W] \geq 100$ μM, the multilamellar model is the only one that leads to acceptable fits of the time-resolved FRET data.

The recovered parameters for these FRET models raise the following points of discussion concerning the fluid phase systems ($T = 60$ °C):

(i) *K_6W is unable to induce phase separation in DPPC/DPPS equimolar membranes in the fluid phase.* Because statistically acceptable fits were obtained with the uniform distribution model with bilamellar (eq 8, $[K_6W] < 80$ μM) and multi-bilayer (eq 9, all samples) geometries (and taking into account that the phase separation model with a trans geometry (eq 10) did not bring any improvement relative to the uniform distribution model with a trans geometry (eq 6)), there is no evidence for peptide-induced phase separation in the lipid bilayers at this temperature. This finding agrees with a microscopy study of

Murray et al.[16] and with NMR work by Franzin and Macdonald[7] who also ruled out the induction of large domains by small basic peptides in mixtures containing acidic lipids. Within each bilayer leaflet, the peptide probably binds to a small number of acidic lipid molecules, and this interaction is insufficient to cause lateral phase separation, such as observed for longer polylysines in phosphatidylcholine (PC)/PS[7] and PC/phosphatidic acid (PA)[4,5] mixtures.

(ii) *K_6W causes local sequestration of negatively charged lipid molecules in the fluid phase.* Even though extensive phase separation is not taking place, data analyses using both the bilamellar and the multilamellar models indicate a gradual increase of the *C* parameter (proportional to acceptor probe concentration). It is probable that small-scale sequestration of negatively charged lipid molecules by the peptide results in an average rarefaction of DPPS molecules from the close vicinity of each donor, as suggested by Roux et al.[51] in their NMR study of PMP1 18−38 interaction with phosphatidylserine. In other words, there is a progressive increased probability of finding DPPC molecules and DPPC-mimicking acceptors in each donor's immediate neighborhood upon increasing the peptide concentration, even though no phase separation occurs. As the region around each donor is the one that FRET probes most efficiently, this would be sensed as an increase in local acceptor concentration, even if the overall concentration is not altered. From simple simulations (Sybyl 6.2, Tripos Associates), the surface area of K_6W in interaction with lipid membranes was calculated as lying between 175 and 195 Å^2, depending on the assumed peptide structure (α-helical or random coil, respectively). This corresponds to the surface area occupied by 2.5−2.8 phospholipid molecules if the area per lipid is in the region of 70 Å^2,[40] and therefore it is an estimate of the maximum number of anionic phospholipids sequestered by the peptide (because of the very short range of the electrostatic interaction). Taking further into account the membrane-bound peptide fraction (75−80%) at the lipid concentration employed in these experiments (0.75 mM), it is possible to predict that all anionic phospholipids present in the liposome outer leaflet should be complexed by the peptide when its total concentration in solution reaches 80−100 μM. Interestingly, this corresponds to the K_6W concentration where the experimental energy transfer efficiency starts to level off with the peptide concentration in the experiments carried out at this temperature (Figure 3B). This is also reflected in a steady increase in the recovered *C* value (which is proportional to surface concentration of acceptors) upon peptide addition to the lipid vesicles until a plateau of $C = 0.45 \pm 0.04$ is reached at 80−100 μM (uniform distribution model, multi-bilayer geometry, Table 2). This *C* plateau level is ∼24% higher than that for $[K_6W] = 0$ μM. In addition to local acceptor enrichment arising from sequestration, this effect could also result from a reduction in the average area per phospholipid molecule upon neutralization with peptide molecules. Using NMR techniques, de Kruijff et al.[17] concluded that there was decreased acyl chain motion in cardiolipin−Lys_{170} complexes relative to pure lipid vesicles (but the lipid remained in the fluid phase). It is thus probable that the observed increase in the *C* parameter as $[K_6W]$ increases stems from a combination of two factors: a reduced donor-to-nearest-acceptor distance (resulting from sequestration of PS by the peptide), together with a smaller average area/lipid molecule in the membrane plane. Of course, it could be argued that, because for multilamellar geometry there would be a third layer of acceptors located at approximately $h_3 = (h_2 +$ one bilayer width$) \cong 74$ Å, which is omitted in our model, the *C* recovered in the analyses would be biased to larger values to compensate for the lack of the third layer of acceptors in the model. We believe this is improbable, because the contribution of FRET to this plane of acceptors would be much smaller due to the R_0 value obtained for this Förster pair and effectively masked by FRET to acceptors located at h_1 and h_2.

(iii) *K_6W bridges two adjacent lipid bilayers, reducing the intermembrane separation to ∼23 Å.* Let us now consider the significance of the variation of the recovered h_2 distance upon increasing $[K_6W]$. As recovered from the multi-bilayer model, h_2 decreases steadily from 67 Å (for $[K_6W] = 0$ μM, Table 2) to a limiting value of ∼40 Å (for $[K_6W] \geq 100$ μM, Table 2). In our multilamellar model, the repeat distance is given by $h_1 + h_2$. Through the use of the h_2 value obtained for $[K_6W] = 0$ μM, this would lead to a repeat distance well in excess of the large repeat distance values for multilamellar vesicles of fluid DPPC at $T = 50$ °C collected in Marsh[40] (60−67 Å). The h_2 value recovered for $[K_6W] = 0$ may thus either reflect a small extent of multilamellarity in the liposome population or possibly be insignificant. Note that the decrease of χ_g^2 in this analysis relative to that assuming a trans geometry is <3% (Table 2). Given that the only formalism that leads to acceptable fits for $[K_6W] \geq 100$ μM is the multilamellar model, we consider that the limiting value obtained in this peptide concentration range reflects the phospholipid organization in the presence of a large amount of peptide, a multi-bilayer structure with repeat distance equal to $h_1 + h_2 \cong 57$ Å. The fact that this distance is smaller than that observed in pure DPPC fluid phase multilamellar vesicles is an indication of the effect of the peptide in bridging adjacent bilayers through electrostatic interaction with anionic lipid molecules from both bilayers and bringing them closer in the process.

For 20 μM $\leq [K_6W] \leq$ 100 μM, the recovered h_2 value is higher than the limiting value. This probably indicates that for these intermediate peptide concentrations, whereas some vesicles remain isolated and therefore unilamellar (possibly due to an insufficient amount of peptide bound to them), other vesicles have already undergone peptide-induced aggregation. The combined increase of *C* and decrease of h_2 upon increasing $[K_6W]$ leads to the increase in FRET efficiency observed in Figure 3 (donor molecules sense on average more acceptors in their vicinity, both in the bilayer plane and in another parallel but increasingly closer plane), which is therefore unrelated to phase separation. The fact that equally good or slightly better fits are obtained when analyzing the data with the bilamellar (eq 8) rather than with the multi-bilayer (eq 9) model may suggest that, for these intermediate peptide concentrations, the effect of the peptide is predominantly limited to aggregation of two bilayers rather than going to the full extent observed for $[K_6W] \geq 100$ μM, that is, formation of multistacked bilayers.

(iv) *Preexistence of large DPPS-rich gel domains (that preferentially exclude the donor and acceptor lipid probes) prevents detection of intermembrane FRET (vesicle aggregation).* The remarkable difference between the decays measured at 45 and 60 °C should be also commented upon. Is there peptide-induced aggregation of the lipid vesicles at $T = 60$ °C but not at $T = 45$ °C? To test this, we carried out right-angle light-scattering measurements of the samples as a function of peptide concentration, at both temperatures (results not shown), and a noticeable increase of the sample turbidity could be detected in both cases. Furthermore, the fact that the decays for $T = 45$ °C are successfully analyzed using a phase separation formalism but not a multi-bilayer formalism does not necessarily exclude peptide-induced vesicle aggregation at this temperature.

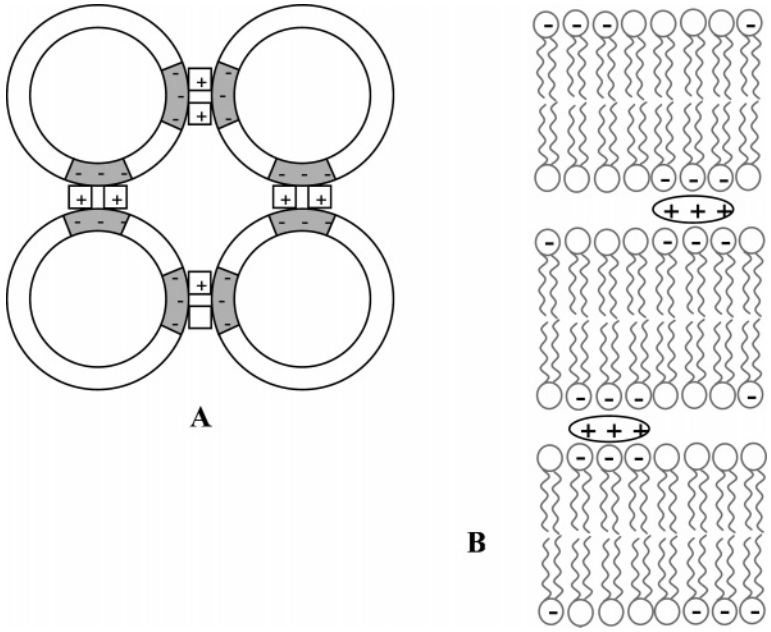

Figure 5. Cartoon representation of possible structures adopted by DPPC/DPPS 1:1 membranes in the presence of ≥ 100 μM K_6W. (A) $T = 45$ °C: There is gel/fluid coexistence at this temperature in the absence of K_6W. Addition of peptide does not change the lateral organization of preexisting domains, which are large on the FRET length scale (>200 Å). The possibility of vesicle aggregation by peptide-mediated adhesion of DPPS-rich, probe-poor gel domains (shaded) is schematically illustrated. (B) $T = 60$ °C: There is no extensive lateral phase separation for all peptide concentrations assayed. K_6W (positively charged) is only able to cluster 2−3 negatively charged DPPS molecules. At the higher peptide concentrations used, a stacked multilayer structure is formed, in which adjacent bilayers are bridged by K_6W molecules. The picture is not drawn to scale.

One should keep in mind that, in this phase-separated system, peptide binding should occur preferentially in the DPPS-rich gel domains rather than in the DPPC-rich fluid phase regions, where both the donor and the acceptor are predominantly partitioned. Therefore, at this temperature, peptide-mediated aggregation of vesicles should be accomplished by the preferential joining of two vesicles through their gel phase regions. In this situation, there would be molecular contact between the vesicles through their respective large gel domains, but most molecules in the fluid phase region of one vesicle are separated from similar regions in the other vesicles present in the aggregate by a distance too large for FRET to occur efficiently. If this is the case, then the FRET decays would probably report a bilayer geometry, because most donor and acceptor probe molecules are located in the fluid phase and would not sense the probes located in other vesicles (Figure 5A). At 60 °C, there is no phase separation, and the peptide molecules are dispersed throughout the whole bilayer, although preferentially sequestering the anionic phospholipids. Therefore, there are no preferential adhesion sites between different vesicles. Aggregation occurs not by joining together two or more vesicles through specific regions but in an arrangement that involves the entire bilayer. In the new geometry, the donor probes are sensitive to acceptors in the same bilayer as well as in adjacent bilayers (Figure 5B).

Concluding Remarks

This study confirms that although a short polylysine peptide is unable to induce lateral phase separation in fluid phase lipid vesicles, apart from short-range clustering of anionic phospholipids, it causes widespread aggregation of DPPC/DPPS vesicles as a consequence of the expected strong electrostatic interaction between the membranes' anionic groups and the positively charged peptide. Furthermore, when peptide binding reaches saturation (at ~ 100 μM in our experiments), there is extensive formation of stacked lipid bilayers, bridged by the basic peptide and with a reduced intermembrane separation of $\sim h_2 - h_1 = 23$ Å.

This work stresses the power of model analysis of time-resolved data over steady-state fluorescence data (or, equivalently, data resulting from integration of fluorescence decays, as shown in Figure 3). Although the latter is much more immediate (it does not require deconvolution analysis, which is far from trivial for complex kinetics such as the FRET models used), it often leads to an incomplete recovery of information regarding the topography and topology of the system under study. This is particularly valid for the FRET interaction. The single data point available from each sample is clearly insufficient for any detailed conclusion. Careful time-resolved analysis (based on adequate kinetic models) is much more powerful, because each sample is associated with a curve of $\sim 10^3$ data points. Different kinetic models (based on distinct topological arrangements) frequently lead to different decay curve shapes, which may or may not fit the experimental curve for physically meaningful values of the parameters. This produces severe restrictions on model acceptability for a given set of samples, and a satisfactory (both statistically and physically) model can often be identified. From this model's parameters (e.g., concentrations, distances) a molecular picture of the system is possible.

Acknowledgment. The authors acknowledge the Fundação para a Ciência e a Tecnologia (Portugal) for financial support, namely, projects and a grant to A.F. (BPD/11488/2002) under the program POCTI.

References and Notes

(1) Johnson, J. E.; Cornell. R. B. *Mol. Membr. Biol.* **1999**, *16*, 217−235.

(2) Cho, W.; Stahelin, R. V. *Annu. Rev. Biophys. Biomol. Struct.* **2005**, *34*, 119−151.

(3) Buckland, A. G.; Wilton, D. C. *Biochim. Biophys. Acta* **2000**, *1483*, 199−216.

(4) Galla, H.-J.; Sackmann, E. *Biochim. Biophys. Acta* **1975**, *401*, 509−529.

(5) Galla, H.-J.; Sackmann, E. *J. Am. Chem. Soc.* **1975**, *97*, 4114−4120.
(6) Buser, C. A.; Kim, J.; McLaughlin, S.; Peitzsch, R. M. *Mol. Membr. Biol.* **1995**, *12*, 69−75.
(7) Franzin, C. M.; Macdonald, P. M. *Biophys. J.* **2001**, *81*, 3346−3362
(8) Hinderliter, A.; Almeida, P. F. F.; Creutz, C. E.; Biltonen, R. L. *Biochemistry* **2001**, *40*, 4181−4191.
(9) Rauch, M. E.; Ferguson, C. G.; Prestwich, G. D.; Cafiso, D. S. *J. Biol. Chem.* **2002**, *277*, 14068−14076.
(10) Gambhir, A.; Hangys-Mihlyn, G.; Zaitseva, I.; Cafiso, D.; Wang, S. J.; Murray, D.; Pentyala, S. N.; Smith, S. O.; McLaughlin, S. *Biophys. J.* **2004**, *86*, 2188−2207.
(11) Hinderliter, A.; Biltonen, R. L.; Almeida, P. F. F. *Biochemistry* **2004**, *43*, 7102−7110.
(12) Arnold, K. In *Handbook of Biological Physics*; Lipowsky, R., Sackmann, E., Eds.; Elsevier/North-Holland: Amsterdam, 1995; p 903−957.
(13) Gad, A. E.; Silver, B. L.; Eytan, G. D. *Biophys. Biochim. Acta* **1982**, *690*, 124−132.
(14) Carrier, D.; Pzolet, M. *Biochemistry* **1986**, *25*, 4167−4174.
(15) Denisov, G.; Wanaski, S.; Glaser, M.; McLaughlin, S. *Biophys. J.* **1998**, *74*, 731−744.
(16) Murray, D.; Arbuzova, A.; Hangyás-Mihályné, G.; Gambhir, A.; Ben-Tal, N.; Honig, B.; McLaughlin, S. *Biophys. J.* **1999**, *77*, 3176−3188.
(17) de Kruijff, B.; Rietveld, A.; Telders, N.; Vaandrager, B. *Biochim. Biophys. Acta* **1985**, *820*, 295−304.
(18) Rand, R. P.; Kachar, B.; Reese, T. S. *Biophys. J.* **1985**, *47*, 483−489.
(19) Kachar, B.; Fuller, N.; Rand, R. P. *Biophys. J.* **1986**, *50*, 779−788.
(20) Coorsen, J. R.; Rand, R. P. *Biophys. J.* **1995**, *68*, 1009−1018.
(21) Loura, L. M. S.; de Almeida, R. F. M.; Prieto, M. *J. Fluoresc.* **2001**, *11*, 197−209.
(22) Gawrisch, K.; Han, K. H.; Yang, J. S.; Bergelson, L. D.; Ferretti, J. A. *Biochemistry* **1993**, *32*, 3112−3118.
(23) Polozov, I. V.; Polozova, A. I.; Molotkovsky, J. G.; Epand, R. M. *Biochim. Biophys. Acta* **1997**, *1328*, 125−139.
(24) Frster, Th., *Z. Naturforsch., A: Phys. Sci.* **1949**, *4*, 321−327.
(25) Van der Meer, B. W.; Coker, G., III.; Chen, S.-Y. S. *Resonance Energy Transfer: Theory and Data*; VCH Publishers: New York, 1994.
(26) Davenport, L.; Dale, R. E.; Bisby, R. H.; Cundall, R. B. *Biochemistry* **1985**, *24*, 4097−4108.
(27) Gill, S. C.; von Hippel, P. H. *Anal. Biochem.* **1989**, *182*, 319−326.
(28) Haugland, R. P. *Handbook of Fluorescent Probes and Research Chemicals*, 6th ed.; Molecular Probes: Eugene, OR, 1996.
(29) Lentz, B. R. In *Spectroscopic Membrane Probes*; CRC Press: Boca Raton, FL; 1988; Vol. I.
(30) Coutinho, A.; Prieto, M. *Biophys. J.* **2003**, *84*, 3061−3078.
(31) McClare, C. W. *Anal. Biochem.* **1971**, *39*, 527−530.
(32) Castanho, M. A. R. B.; Santos, N. C.; Loura, L. M. S. *Eur. Biophys. J.* **1997**, *26*, 253−259.
(33) Loura, L. M. S.; Fedorov, A.; Prieto, M. *J. Phys. Chem. B* **2000**, *104*, 6920−6931.
(34) Lakowicz, J. R. *Principles of Fluorescence Spectroscopy*, 2nd ed.; Plenum/Kluwer: New York, 1999.
(35) Santos, N.; Prieto, M.; Castanho, M. A. R. B. *Biochim. Biophys. Acta* **2003**, *1612*, 123−135.
(36) Davenport, L. *Methods Enzymol.* **1997**, *278*, 487−512.
(37) Loura, L. M. S.; Fedorov, A.; Prieto. M. *Biochim. Biophys. Acta* **2000**, *1467*, 101−112.
(38) Eaton, D. F. *J. Photochem. Photobiol., B* **1988**, *2*, 523−531.
(39) Luna, E. J.; McConnell, H. M. *Biochim. Biophys. Acta* **1977**, *470*, 303−316.
(40) Marsh, D. *Handbook of Lipid Bilayers*; CRC Press: Boca Raton, FL, 1990.
(41) Chattopadhyay, A.; London, E. *Biochemistry* **1987**, *26*, 39−45.
(42) Kleinschmidt, J. H.; Marsh, D. *Biophys. J.* **1997**, *73*, 2546−2555.
(43) Vivian, J. T.; Callis, P. R. *Biophys. J.* **2001**, *80*, 2093−2109.
(44) Montich, G.; Scarlata, S.; McLaughlin, S.; Lehrmann, R.; Seelig, J. *Biochim. Biophys. Acta* **1993**, *1146*, 17−24.
(45) Mosior, M.; McLaughlin, S. *Biochim. Biophys. Acta* **1992**, *1105*, 185−187.
(46) Ben-Tal, N.; Honig, B.; Peitzsch, R. M.; Denisov, G.; McLaughlin, S. *Biophys. J.* **1996**, *71*, 561−75.
(47) Kim, J.; Mosior, M.; Chung, L. A.; Wu, H.; McLaughlin, S. *Biophys. J.* **1991**, *60*, 135−148.
(48) Loura, L. M. S.; Fedorov, A.; Prieto, M. *Biophys. J.* **2001**, *80*, 776−788.
(49) Loura, L. M. S.; Fedorov, A.; Prieto, M. *Biochim. Biophys. Acta* **2001**, *1511*, 236−243.
(50) de Almeida, R. F.; Loura, L. M.; Fedorov, A.; Prieto, M. *Biophys. J.* **2002**, *82*, 823−834.
(51) Roux, M.; Beswick, V.; Coïc, Y.-M.; Huynh-Dinh, T.; Sanson, A.; Neumann, J.-M. *Biophys. J.* **2000**, *79*, 2624−2631.